JMEPEG (2019) 28:3341–3348
https://doi.org/10.1007/s11665-019-04119-7

1059-9495/$19.00

Mechanism of Nonequilibrium Formation of Novel Interface Structures in Explosive Welding

Yanshu Fu and Mingzhen Shi

(Submitted September 13, 2018; in revised form January 7, 2019; published online June 3, 2019)

Novel structures are commonly observed in explosive welding products. This paper presents the nonequilibrium mechanism of the welding interface. A theoretical model was established first to deduce the motion equation of the rapid accelerated flyer plate. Numerical simulations of the welding interface were carried out with the smooth particle hydrodynamic method. Both the theoretical and numerical results were compared with experimental phenomena and showed that under the very rapid application of an impact load usually associated with high-strength plastic deformation, a significant strain rate, and temperature rise, the material volumes of the welding interface are in the viscoelastic state and prone to rotation, detrusion, and dilatation. In addition, the extreme values from the nonequilibrium development of the interface structure are a consequence of the competition between the loading and unloading stress waves during the explosive welding process.

Keywords explosive welding, nonequilibrium, thermomechanics, wavy interface structure

1. Introduction

Explosive welding (EXW) is a joining method comprising a solid-state welding process using a controlled explosive detonation on the surface of a metal. The detonation produces a high-velocity jet that removes the impurities on the metal surface. Experimental observations have shown that the EXW interface always presents periodic wavy structures (macro or micro) with a well-defined wavelength and amplitude. The wave formation due to EXW has been extensively investigated with empirical and numerical models (or mechanisms) over the past five decades, yet understanding of the mechanism remains incomplete. Theories for the wave formation mechanism fall within the following categories: indentation, flow instability, vortex shedding, and stress waves (Ref 1).

Among the various proposed mechanisms, instability owing to large tangential velocity variations near the interface has received significant attention. Further support for the proposition that wave formation results from instability has been provided by comprehensive experimental and computational studies on EXW in the last two decades (Ref 2-9). Plaksin et al. (Ref 2) attributed the wave formation mechanism to regular instabilities that are induced by oscillating detonation waves and transmitted through the interface of the impact materials. Mousavi and Al-Hassani (Ref 3) argued that the surface disturbances both ahead and behind the collision point are caused by successive interference from rarefaction waves in both plates and multilayered welding; they proposed that the waves are generated in front of the collision point, while the vortices are created subsequently. Ben-Artzy et al. (Ref 4) established a Kelvin–Helmholtz instability mechanism for the formation of interface waves where reflected shockwaves are the source of interference at the welding interface. In the case of dissimilar materials, the conditions of the Richtmyer–Meshkov and Kelvin–Helmholtz instabilities and, at an appropriate density ratio, Rayleigh–Taylor instability are satisfied. However, if two layers of the same metal are in tight contact, the interface should be stable (Ref 5). Drennov et al. (Ref 6) developed a numerical simulation to show that the development of perturbations during passage of an oblique shockwave through the interface of identical metals is most probably due to the presence of a small micro-gap. Their calculation also yielded a spectrum of perturbation wavelengths. The effect of the initial gap on the impact angle that sets the relationship between the collision point velocity and weld propagation velocity was also discussed by Mousavi and Al-Hassani (Ref 3). Nassiri et al. (Ref 7, 8) determined that there are two different types of shear flow instability: temporal and spatial. They (Ref 7) performed a quantitative temporal linear stability analysis to investigate whether the interfacial wave morphology can be the signature of a shear-driven high-strain-rate instability of a perfectly plastic material undergoing jet-like deformation near the interface. Raoelison et al. (Ref 9) also believed that the disturbance amplifies in time but not in space.

Besides, features of interface in impact welding were researched by smoothed particle hydrodynamics (SPH) method in several papers. The composition of the metal jet (Ref 10, 11), the temperature distribution (Ref 12) and the historical changes of shear stress, effective plastic strain of materials (Ref 13) were developed by SPH.

Most of the previous studies considered the mechanical processes of the wavy interface based on the continuum mechanics theory and ignored the thermodynamic process. In fact, the formation and development of the welding interface is a nonequilibrium process; several experimental observations in the literature (Ref 2-9) and numerical simulations (Ref 10-13) have revealed that high-velocity collisions generate shear instability with a large strain and changes in the grain size and shape. Thus, the aim of this study was to explain the

Yanshu Fu and **Mingzhen Shi**, School of Mechanical & Electrical Engineering, Nanchang University, Nanchang 330031, China. Contact e-mail: yshfu@ncu.edu.cn.

formation mechanism of the interface structure based on the nonequilibrium/irreversible physical theory, which considers not only the mechanical behavior but also the thermal effects.

The remainder of this paper is organized as follows. Section 2 establishes the nonequilibrium motion equation for the volume elements of the EXW interface. Section 3 presents the numerical model for analyzing the nonequilibrium behavior of the volume elements based on the smoothed particle hydrodynamics (SPH) method, which furnishes a foundation for the following discussion on the interface structure. Section 4 combines the numerical analysis and experimental phenomena to discuss the coupling effect of the thermal and mechanical responses during the nonequilibrium process. Section 5 discusses the extreme values of the wavy interface.

2. Mechanism of the Nonequilibrium State for the Interface

The EXW process can be described by the theory of interaction between the detonation wave and flyer plate (Ref 14). The motion-specific parameters can be expressed as shown in Fig. 1. The detonation wave D_J acts on the upper surface A_1 of the flyer plate and drives it to the turning angle θ_2 to introduce the refracted wave T_1T_2, simultaneously, a reflected wave RT_1 was introduced. Then, the refraction wave T_1T_2 is reflected on the lower surface of the flyer plate, the refracted wave acts on the free surface A_2 to get the turning angle θ_3 and reflects the rarefaction wave R' at T_2. This rarefaction wave interacts with the surface T_1B_1 to gradually obtain the same turning angle θ_3. The refraction wave T_1T_2 is usually not vertical or overlapping the lower surface of the flyer plate, so its effect can be resolved into two parts: along the flyer plate and perpendicular to it. Thus, the flyer plate can receive the normal acceleration a_n and tangential acceleration a_τ.

According to Fig. 1, the EXW process intensively accelerates the flyer plate to the nonequilibrium state. Consider an infinitesimal tetrahedron formed by three surfaces parallel to the coordinate planes and one normal to the unit vector, as shown in Fig. 2 (Ref 15, 16). The unit normal vector is $\vec{n}$, and the surface force per unit area is $\overset{n}{T}$. As existing acceleration features, the inertial force and body force can be represented by $\Delta m\ddot{u}$ and Δmg_i $(i = 1, 2, 3)$, respectively, where the number of dots represents the differentiation order of time. Stress components σ_{ij} $(i, j = 1, 2, 3)$ act on three surfaces $\Delta A_j = \Delta A_n n_j$ that are parallel to the coordinates, where $n_j = (1, 2, 3)$ is the unit vector normal to the surface ΔA_n. By interchanging the dummy indices i and j, the equation of motion can be expressed as

$$\overset{n}{T}_i \Delta A_n + \Delta mg_i = \sigma_{ij} n_j \Delta A_n + \Delta m\ddot{u}_i, \quad i = 1, 2, 3 \qquad \text{(Eq 1)}$$

where ρ is the mass density and $\Delta m = \rho \Delta V$. Equation 1 can be rewritten as

$$\overset{n}{T}_i = \tau_{ij} n_j \qquad \text{(Eq 2)}$$

$$\tau_{ij} = \sigma_{ij} + \rho(\ddot{u}_i - g_i)\gamma_j, \quad i,j = 1, 2, 3 \qquad \text{(Eq 3)}$$

where $\gamma_j = \Delta V / \Delta A_n$.

In Eq 3, once there is an acceleration that differs from g_i on the infinitesimal tetrahedron $\ddot{u}_i \neq g_i$. At this time, if $\lim \gamma_i = \Delta V / \Delta A_n \to 0$, then Eq 3 deteriorates into $\tau_{ij} = \sigma_{ij}$, which cannot reveal the features of impact load with a considerable loading speed. While as shown in Fig. 1, in explosive welding process, the welding plates were severely driven to a remarkable acceleration, $\ddot{u}_i \neq g_i$, even $|\ddot{u}_i| \gg |g_i|$. Because Eq 3 was established for describing the element motion of welding plates, there should be the change rate of the element volume to its surface area $\gamma_i \neq 0$, then $\tau_{ij} \neq \sigma_{ij}$. As shown in Fig. 1, during the EXW process, because $\ddot{u}_i \neq g_i$ and $\gamma_i \neq 0$, then $\tau_{ij} \neq \sigma_{ij}$, which fundamentally changes the boundary condition and stress transformation. Therefore, the surface force acting on the volume element ΔA should no longer be independent of the body force, while it should be proportional to the mass Δm in ΔV.

The driven kinetic energy per unit is yielded by

$$W = \int F \mathrm{d}x = \int mv \frac{\mathrm{d}v}{\mathrm{d}x} \mathrm{d}x = \int I_d \ddot{u}_i \mathrm{d}t \qquad \text{(Eq 4)}$$

The driven energy of volume element ΔV is determined by the impulse, acceleration, and acting time. It is proportionally converted to the activation energy for the interface structure

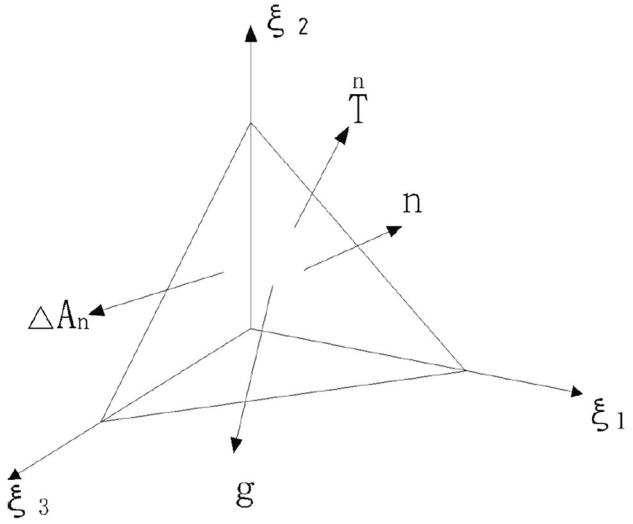

Fig. 1 Detonation acting on a metal plate

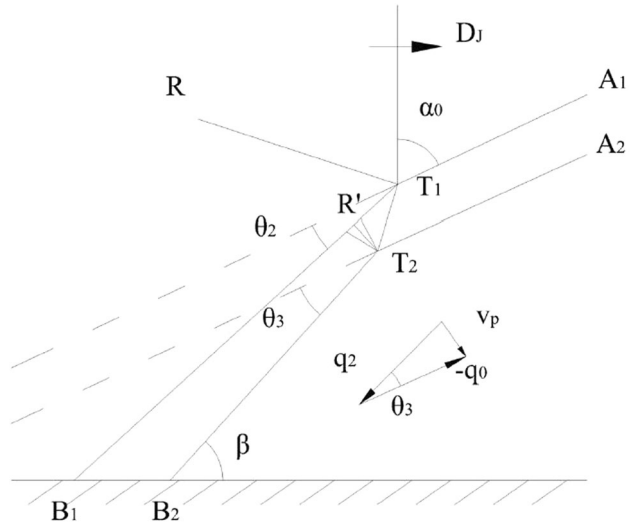

Fig. 2 Free-body diagram for an element

(Ref 17), where the difference between zones results in variability of the welding interface structure. The presence of all features such as streaks, bumps, curls, and even embedded features in both the cross section and longitudinal section is the effect of integrating Eq 3 and 4 in three directions.

To demonstrate the structural response of the welding interface caused by the nonequilibrium behavior of volume elements, the welding interface was cut along the longitudinal direction, as shown in Fig. 3(a). After sanding, polishing, and etching, a digital microscope was used to take images, as shown in Fig. 3(b) and (c). Both images show black-and-white strings representing 245 carbon steel and 304 stainless steel, respectively. Combined with the cross-sectional structure shown later in Fig. 5(b), the nonequilibrium behavior of the material volume is clearly revealed, which verifies Eq 3 and 4. Furthermore, the streaks, bumps, twists, and even embedded features at the welding interface indicate remarkable development of the nonequilibrium features of volume elements over the whole vertical section during the welding process.

As given by Eq 2, although the body force ρg_i and inertia force $\rho \ddot{u}_i$ are in the centroid of the material element and the components of stress σ_{ij} are symmetric, the reciprocal of γ_i, $\frac{1}{\gamma_i}$, has the dimension of the strain gradient. Thus, τ_{ij} is not symmetrical; this results in a torque $M_i = \int \rho(\ddot{u}_i - g_i)\gamma_i \mathrm{d}v$ being distributed on the volume element and causes micro-volume rotation. Actually, the symmetric stress tensor $\tau_{ij} = \tau_{ji}$ is based on the equilibrium state of the element. However, during the explosive welding process, elements were accelerated to nonequilibrium state; therefore, their stress tensors are naturally unsymmetrical. This explains well the crimped, staggered, and even mutually embedded features of the interface.

As shown in Fig. 1, due to the severe plastic deformation and high strain rate, the metal usually acts as a viscoplastic fluid under the action of a detonation wave. Simultaneously, both the nonequilibrium force and distributed moment provide the driving force for the motion and rotation of the liquid metal fluid, which also explains the instability of the fluid motion. Therefore, the novel structures of the welding interface are the inevitable result of the rotation, detrusion, and dilatation of volume elements under the action of the nonequilibrium force and moment. Hence, the formation of novel structures at the welding interface is clarified in this section. However, depicting the characteristics of novel structures remains difficult. In order to do so, numerical simulations were carried out on the EXW interface with the SPH method for comparison with the experimental results.

3. Numerical Model for the Welding Interface Nonequilibrium Behavior by SPH

Numerical analysis of EXW by SPH has been used to reveal the formation mechanism of the wavy interface during impact welding (Ref 10-13). Good quantitative agreement has been obtained between experimentally observed wavy interface morphologies and the simulations. All these studies proved that the numerical analysis is a powerful tool for studying the formation mechanism of the intermediate layer at impact-welded interfaces.

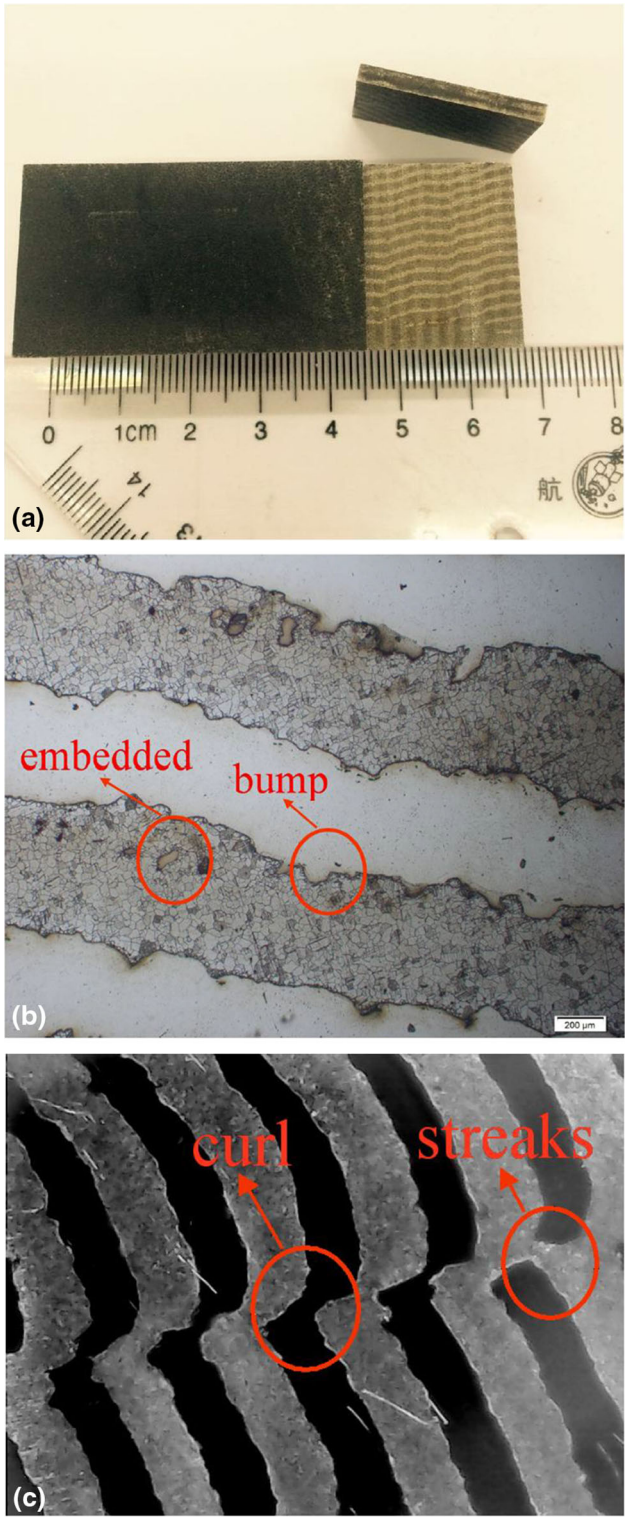

Fig. 3 Longitudinal section of the welding interface: (a) texture characteristics in the longitudinal section and (b, c) digital microscopy images

In this study, the impact welding process was numerically modeled by SPH in the software AUTODYN-2D. The particle size was 20 μm. In all cases, 2D calculation models were selected. The flyer and base plates in the model were set to thicknesses of 3 and 18 mm, respectively, and a length of 20 mm for both. Nishiwaki et al. confirmed that the wavy

interface morphology could be quantitatively predicted with the SPH method based on the impact angle and impact velocity (Ref 10, 11). Thus, the initial conditions were set to an initial velocity of 500-800 m/s and impact angle of 5°-25°. The flyer and base plates were made of SS304 stainless steel and Q245 steel, respectively. Table 1 presents the physical values for the state parameters used in the equation.

Because the Johnson–Cook equation takes into account the effect of temperature, plastic strain, and plastic strain rate on the flow stress, it was used as the strength model in the simulation (Ref 3, 12, 18). The temperature transformation was shown in the process (Ref 3). In the Johnson–Cook constitutive equation, the flow stress is given as

$$\sigma = (A + B\varepsilon^n)[1 + C\ln\dot{\varepsilon}_p][1 - (T^*)^m] \quad \text{(Eq 5)}$$

where σ is equal to $\overset{n}{T}$ in Eq 2, ε is the equivalent plastic strain, $\dot{\varepsilon}_p$ is the plastic strain rate for $\dot{\varepsilon}_0 = 1.0/s$, T^* is the homologous temperature $T^* = (T - T_{\text{room}})/(T_{\text{melt}} - T_{\text{room}})$, and T is the absolute temperature for $0 \leq T^* \leq 1.0$. The five constants are A, B, C, m, and n. The first quantity in parentheses is the stress as a function of the strain for $\dot{\varepsilon}_p = 0$ and $T^* = 0$. The expressions in the second and third sets of brackets represent the effects of the strain rate and temperature, respectively. At the melting temperature $T^* = 1$, the stress approaches zero for all strains and strain rates. The five material constants and melting temperature T_{melt} are presented in Table 1.

Based on the SPH numerical model shown in Fig. 4(a), the interface characteristics in the numerical simulation were implemented with an impact angle of 20° and initial velocity of 850 m/s between the flyer and base plates during the EXW process. According to the principle of EXW, the most obvious feature was the appearance of a jet and the formation of a wavy interface during the oblique collision (a wavy interface is the main characteristic of EXW materials), as shown in Fig. 4(b). Because the density difference between the flyer and base plates was very small or even zero, the metal jet was composed of both metals. This agrees with other simulation results (Ref 11, 14) and verifies the rationality of the simulation model shown in Fig. 4(a).

4. Development of the Nonequilibrium Behavior of the EXW Interface

In order to clarify the decisive effects of the nonequilibrium thermodynamic behavior of interface volume elements on the welding interface, the simulation results for the morphological characteristics and temperature field were further analyzed and compared with the experimental results. The influence of the development of the nonequilibrium behavior of volume elements on the actual structural characteristics of the interface was examined.

Table 1 Material parameters of the Johnson–Cook constitutive equation

Material	A, MPa	B, MPa	n	C	m	T_{melt}, K
Q245R	244.8	899.7	0.94	0.0391	0.757	1811
304	454	1962	0.75	0.1732	0.699	1790

As shown in Fig. 5(a), the wavy welding interface had a clear vortex structure. The wavy structure was inclined to one side with left–right asymmetry, which makes the peaks and valleys develop into a swirling shape. The interface material twisted and locally rolled within the vortex, similar to a fluidic motion. This is a clear characteristic of the widely known Kelvin–Helmholtz instability, which can be regarded as the result of the action of a nonequilibrium distributed moment. As shown in Fig. 5(b), the experimental results for the topography of the welding interface showed a remarkable wavy structure, the corresponding front and back vortices were clearly visible, and the feature of rolling to one side was quite comparable.

Figure 6(a) shows the interface temperature field at t = 6 μs. The increase in temperature was highly localized at the collision interface, which corresponds to the region where a vortex was observed at the welding interface. The rising temperature during the EXW process consisted of three components. First, the flyer plate was driven by the detonation to a Hugoniot equilibrium at very short time after the passage of the wave front, and both the pressure and temperature reached certain values. Second, the pressure of the new Hugoniot equilibrium increased to a higher state during the impact process, as did the temperature. Third, because of the high-strength plastic deformation, which always involves the dissipation of mechanical energy, each micro-volume of the material underwent an instantaneous temperature rise as an adiabatic process in a narrow zone during EXW. As shown in Fig. 6(a), the temperature at the collision interface was almost

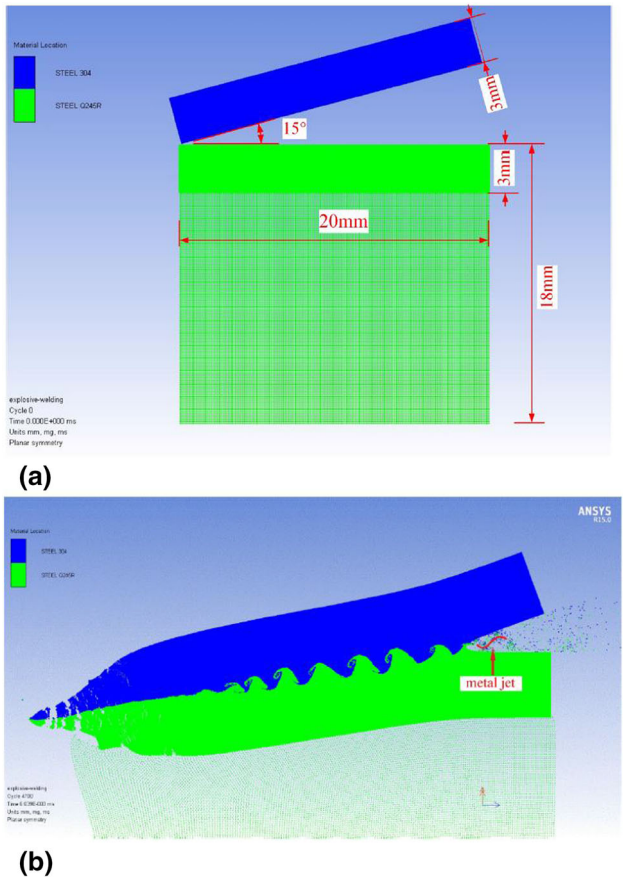

Fig. 4 Numerical simulation of explosion welding: (a) numerical model and (b) the welding interface and jet

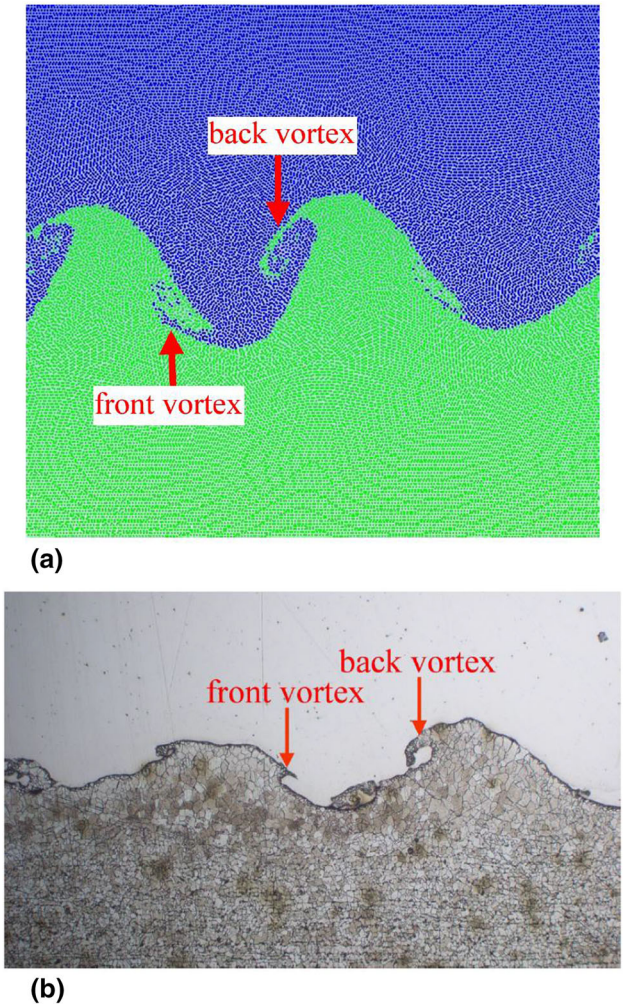

Fig. 5 EXW interface: (a) simulation result and (b) experimental phenomena

2000 K and much higher than that in other regions. Thus, the temperature change caused by the dynamic deformation can be deduced to be the dominant component. Plastic deformation generates heat, and a very rapid load application is usually associated with a localized plastic flow with a large temperature gradient and anisotropic effects. Thus, the simulation results confirmed the effects of plastic deformation and rapid load application.

At present, no reliable experimental measurements of the interface temperature have been published until now. Moreover, such an experiment is likely to be very complicated. The structural evolution of the welding interface during EXW is related to the temperature of the material volume elements and the deformation history of these areas. Thus, some insight into the initial temperature distribution can be obtained indirectly from metallographic studies of welded samples, as shown in Fig. 6(b). Here, the welded materials were divided into three zones. In the first zone near the interface, the severe plastic deformation with a high strain rate heated the material to a remarkable high temperature, even melting point locally. In the second zone at some distance from the collision plane, both the deformation and temperature were significant, but to an extent lower than the first zone. The temperature in this zone gradually decreased in the direction toward the third zone. In the third zone, the material was only slightly deformed and heated by the propagation of shockwaves.

In the most severely strained areas near the interface, the heating rate was on the order of 10^9 K/s, localized crystal grain breaking occurred. While the volume of the local melting area was significantly smaller than that of the bulk metal, the subsequent high rate cooling occurred was 10^7 K/s (Ref 12, 19) by heat transferring from the interface area to less deformed layers, which led to the material quenching into vortices. As shown in Fig. 6(b), the first zone was full of very fine grains resulting from the severe plastic deformation during the EXW process and recrystallization after the heat treatment.

In the second zone, the plastic strain rapidly decreased with distance away from the interface, and the temperature rise was proportional to the strain. After a short time, the high strain rate deformation in the first zone transmitted the heat associated with the plastic work to the second zone and introduced another temperature rise. This even resulted in aging heat treatment over the material volume. Therefore, the second zone displayed relatively large-sized isometric crystals.

Compared with the second zone, there was nearly no distinct plastic deformation and temperature distribution in the third zone. Thus, the crystal size decreased instead. In order to quantify the grain size of the three zones, average grain diameter was calculated per unit length (Ref 20). Grain diameter was defined as the reciprocal of grain number per unit length by counting grain number across a line. Figure 6(c) shows the variation of average grain diameter with different zones, respectively. The average grain sizes are approximately 13.0 μm in first zone, 23.0 μm in second zone, and 16.0 μm in third zone. Besides, Fig. 6(d) shows the comparison between the crystal size in the third zone and that in original material. Both of the average crystal diameters are about 16 μm; therefore, the crystal size in the third zone did not change actually. In general, the different grain sizes were caused by the comprehensive effect of different levels of plastic deformation and temperature distribution (Ref 21).

More importantly, the small-sized crystals in the first zone and large-sized crystals in the second zone, as shown in Fig. 6(b), directly prove $\gamma_i = \Delta V_n / \Delta A_n \neq 0$. Thus, the nonequilibrium force and distributed moment must act on each material volume element where the material underwent changes in the crystal size and shape, even during the phase transition in the EXW process. Now, simple geometric interpretations can be given for $\gamma_i > 0$, $\gamma_i < 0$, and $\frac{1}{\gamma_i} \neq 0$ as grain inflation, breaking, and elongation, respectively. Therefore, the rotation, detrusion, and dilatation seem to result from the nonequilibrium development of welding elements.

5. Extreme Values for the Nonequilibrium Thermodynamic Behavior of the Interface

The nonequilibrium state means that the structural development of volume elements does not have a single value. Nearly, all of the literature (Ref 1-15) has not quantitatively analyzed the wavy interface structure but only described it qualitatively. Thus, the question naturally arises of how to determine extreme values when the welding parameters are given, i.e., $G(c)$. Sih (Ref 15) revealed that the nonequilibrium/irreversible solutions are bounded by the equilibrium/irreversible process and possess

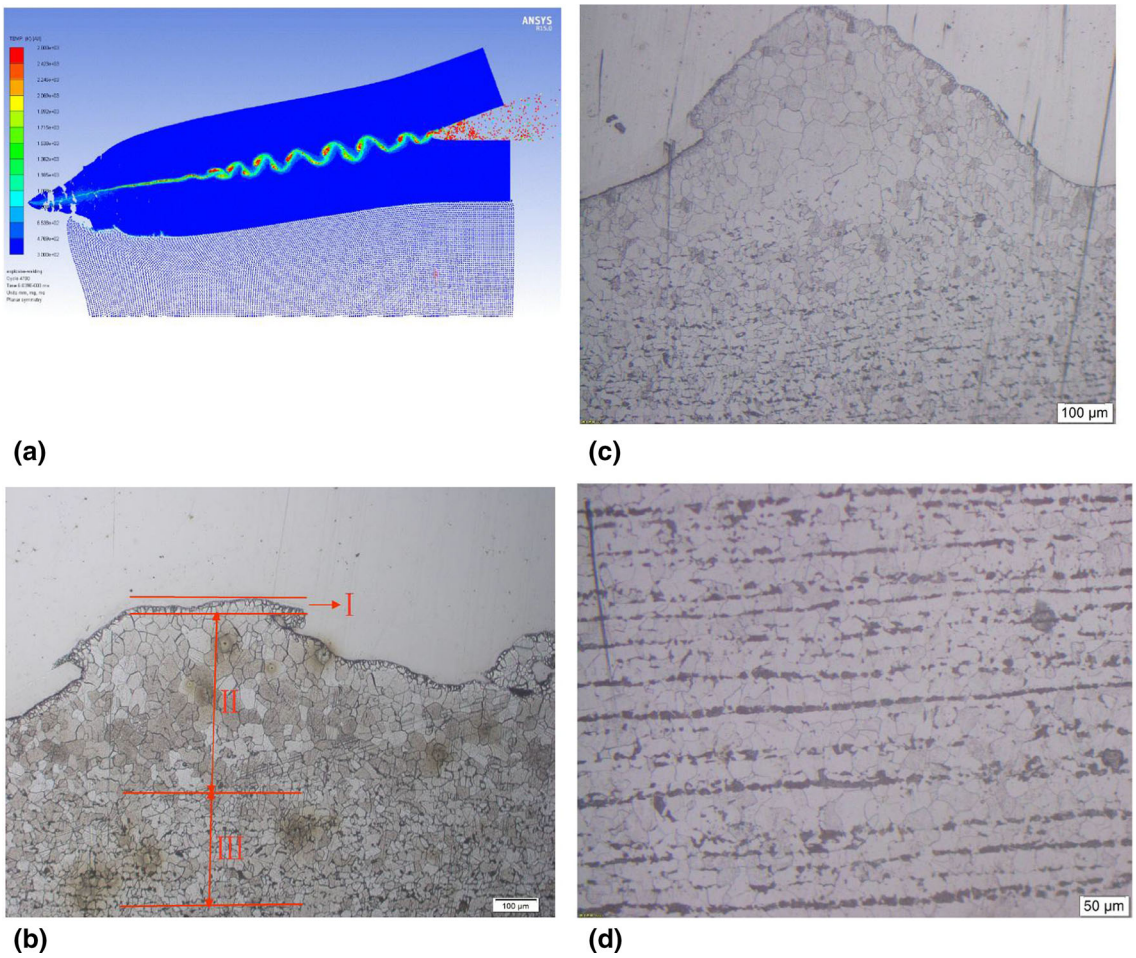

Fig. 6 Effects of the temperature distribution in the welding interface: (a) temperature distribution in the welding interface, (b) variation in the grain size with distance away from the welding interface, (c) the average grain size varied with the location zone, and (d) the comparison of crystal size in third zone with that in original material (the left is the crystal size in third zone, and the right is that in the original material)

definite limits that are determined by both the initial conditions and loading history.

The above sections systematically discussed the formation and development of nonequilibrium behavior of infinitesimal elements in interface under the impact loading during the EXW process. The inevitability of $\gamma_i = \Delta A_n/\Delta V_n \neq 0$ was clarified, which revealed the rotation, detrusion, and dilatation of interface volume elements under the actions of a nonequilibrium force and the corresponding distributed moment. The extreme values for the structural development of the interface are discussed below.

The quality and morphology of the interface depend on the collision angle, impact velocity, and properties of the materials and geometry of the welding plates (Ref 3). Therefore, the collision angle and impact velocity are the decisive factors for detecting the structural development of the EXW interface for welding two plates, which were determined for SS304 stainless steel (3 mm thick) and Q245 steel (18 mm thick) in Sect. 2.

The collision angle plotted against the impact velocity in a rectangular coordinate system forms the EXW window. Based on it, Athar and Tolaminejad (Ref 22) predicted the proper welding parameters for Al-Cu couples, and Mousavi and Sartangi (Ref 23) determined the operational parameters for cladding titanium to stainless steel plates. Nassiri et al. (Ref 18) took advantage of the arbitrary Lagrangian–Eulerian (ALE) technique in a numerical simulation to study the effect of the impact velocity (V_F) and impact angle (β) and capture the wavy interface.

In this study, a series of simulations were performed to detect limitations for the development of nonequilibrium behavior. The impact velocity was varied from 500 m/s to 740 m/s in increments of 80 m/s, and the impact angle was varied from 8° to 22°. The numerical model shown in Fig. 4 was used to carry out a series of calculations for the interface structure with different collision velocities and impact angles, and the variations in the interface structure were used to explain the extreme values of nonequilibrium mechanical behavior.

Figure 7(a) reveals the characteristics of the interface wave with a changing collision velocity at the collision angle β of 20°. The interface morphology changed from straight to wavy and from horizontal to vertical with an increasing collision velocity. Similarly, Fig. 7(b) reveals the characteristics of the interface wave with a changing collision angle at the impact velocity V_F of 600 m/s. The wavelength and amplitude of the interface wave changed significantly with the collision angle between the flyer and parent plates during the impact welding.

As the specific impact velocity and collision angle increased, the interface structural features changed from a straight line to a sine wave and then developed to a vortex wave. When V_F and β reached larger values (V_F=740 m/s,

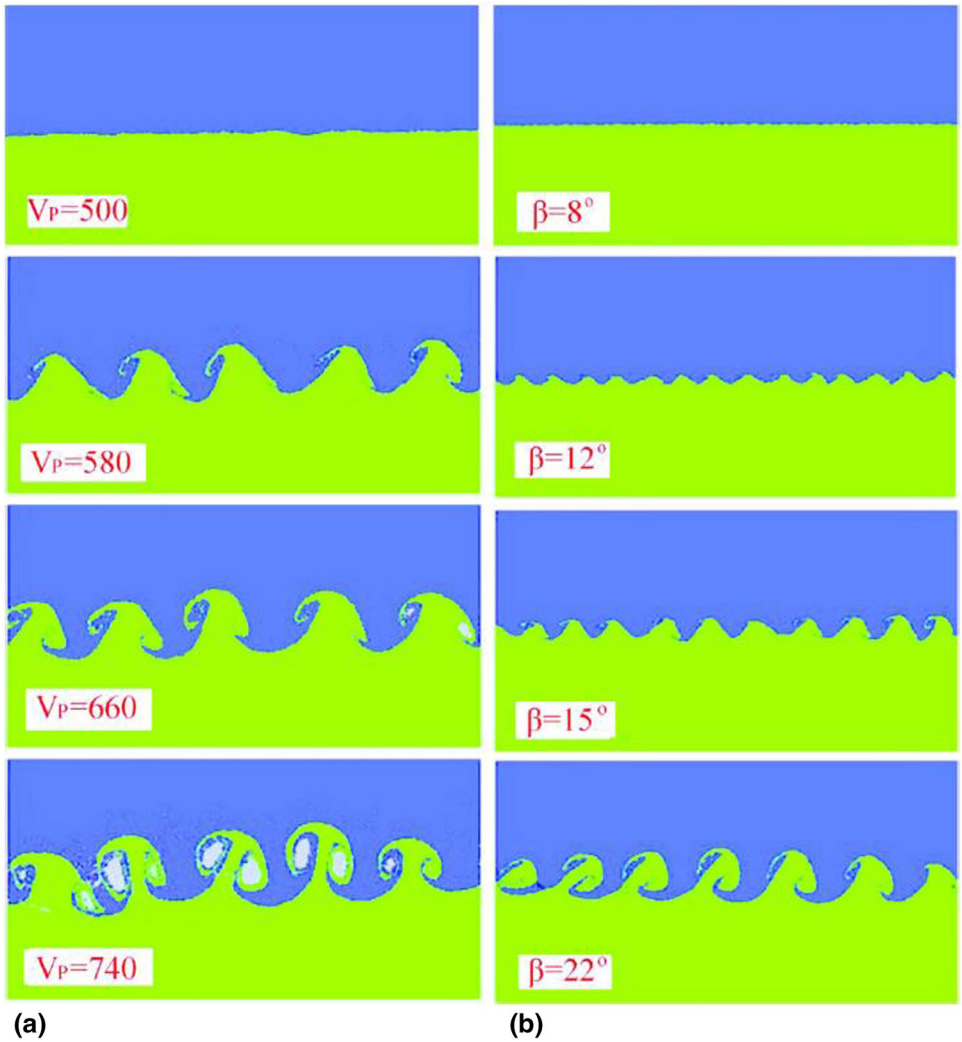

Fig. 7 Characteristics of the EXW interface with varying parameters: (a) varying impact velocity when $\beta = 20°$, (b) varying collision angle when $V_F = 600$ m/s

$\beta = 22°$), the interface peak and valley showed a typical mushroom-shaped structure. Because the collision velocity between the base and flyer plates was higher, the corresponding collision energy greatly increased, and the nonequilibrium force was enhanced. On the one hand, this caused very rapid plastic deformation with a high strain rate and localized temperature rise near the interface, which had the comprehensive effect of weakening the shear resistance and enhancing the flow behavior of the metals. On the other hand, this expanded the area of the metal plastic deformation, which increased the material volume of the zone involved in the flow. The analysis combined with Eq 3 indicated that $\overset{n}{T}_i$ was larger for a high specific impact velocity or large collision angle, while σ_{ij} was smaller when the rate of increase in the temperature was high. Thus, the second term on the right side of Eq 2 should have a corresponding response; this can be expressed as the increases in $\rho(\ddot{u}_i - g_i)\gamma_i$ and the corresponding distributed moment. Therefore, the tumbling feature of the wavy interface is far more remarkable.

Wavelengths of wavy interfaces under a series of specific impact velocities and collision angles were collected from numerical calculations to plot the curves shown in Fig. 8. As the impact velocity and collision angle increased, the extreme value of the wavelength tended to a constant. This is because the development of nonequilibrium behavior is the result of integrating $\rho(\ddot{u}_i - g_i)$ over time. However, after a short time, the unloading wave from the boundary reached the welding interface; this caused the nonequilibrium force $\overset{n}{T}_i$ to be unloaded, so the corresponding strain rate and temperature decreased. According to Eq 4, decreasing the strain rate and temperature significantly increases σ_{ij}. Thus, the response of the second term on the right side of Eq 2 decreased and gradually decayed to zero. Therefore, the extreme values that develop from nonequilibrium are the consequence of competition between the loading and unloading stresses during the EXW process. The amplitude is surely bounded by the thicknesses of the welding couples. Therefore, its limitation did not need to be detected.

6. Conclusions

In this study, theoretical analysis, experimental research, and numerical calculations were used to systematically discuss the nonequilibrium mechanism for the formation and development

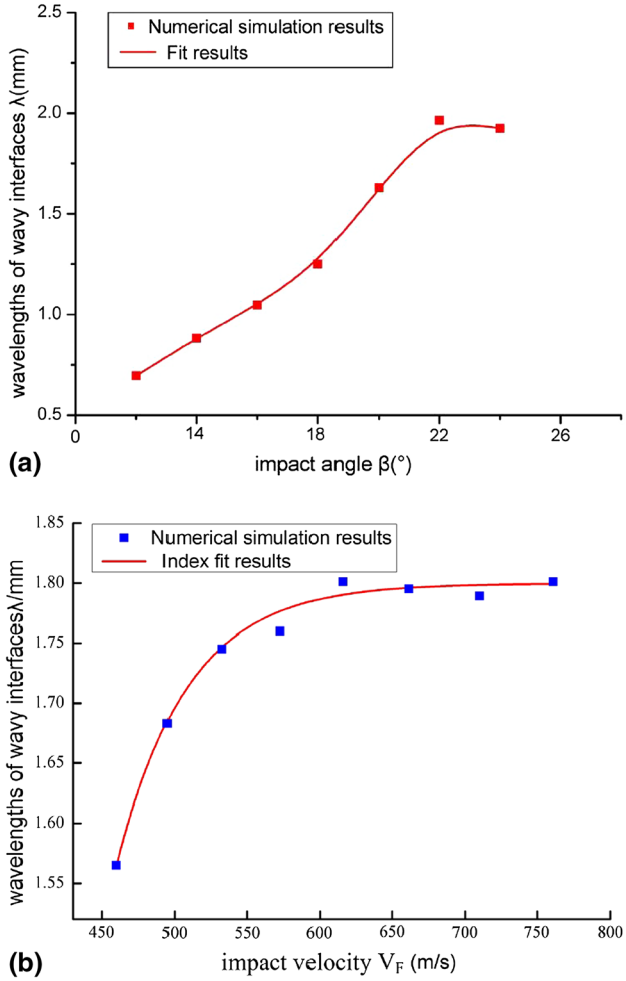

Fig. 8 Wavelength with a varying impact angle (a) and collision velocity (b)

of novel interface structures. The following conclusions were made:

During the EXW process, the flyer plate is driven to the nonequilibrium state by the detonation wave, and the nonequilibrium stress distribution and strain gradient near the welding interface cause rotation, detrusion, and dilatation of volume elements.

Both the experimental and numerical results showed that the interface structure is the comprehensive effect of the thermal response and mechanical deformation of volume elements and has typical nonequilibrium thermomechanical characteristics.

The extreme values of nonequilibrium thermodynamic development are the consequence of competition between the loading and unloading stress waves during EXW and are determined by the initial and boundary conditions and loading history.

Acknowledgments

This work was supported by the National Natural Science Foundation of China (Grant No. 11662010) and Natural Science Foundation of Jiangxi Province, China (Grant No. 20171BAB206036).

References

1. B.H. Shao and K. Zhang, *The mechanism and engineering application for the explosive welding*, Dalian University of Technology Press, Dalian, 1987 (Chinese)
2. I. Plaksin, J. Direito, D. Braga et al., Novelties in Physics of Explosive Welding and Powder Compaction, *Mater. Sci. Forum*, 2008, **566**, p 135–140
3. A.A. Akbari Mousavi and S.T.S. Al-Hassani, Numerical and Experimental Studies of the Mechanism of the Wavy Interface Formations in Explosive/Impact Welding[J], *J. Mech. Phys. Solids*, 2005, **53**, p 2501–2528
4. A. Ben-Artzy, A. Stern, N. Frage, V. Shribman, and O. Sadot, Wave Formation Mechanism in Magnetic Pulse Welding[J], *Int. J. Impact Eng.*, 2010, **37**, p 397–404
5. O.B. Drennov, A.L. Mikhailov, P.N. Nizovtsev et al., Instability of an Interface Between Steel Layers Acted Upon by an Oblique Shock Wave[J], *Int. J. Impact Eng.*, 2005, **32**, p 161–172
6. O.B. Drennov, A.I. Davydov, A.L. Mikhailov et al., Shear Instability at the "Explosion Product-Metal" Interface for Sliding Detonation of an Explosive Charge[J], *Int. J. Impact Eng.*, 2005, **32**, p 155–160
7. Ali Nassiri, Brad Kinsey, and Greg Chini, Shear Instability of Plastically-Deforming Metals in High-Velocity Impact Welding, *J. Mech. Phys. Solids*, 2016, **95**, p 351–373
8. Ali Nassiri, Greg Chini, and Brad Kinsey, Spatial Stability Analysis of Emergent Wavy Interfacial Patterns in Magnetic Pulsed Welding, *CIRP Ann.-Manuf. Technol.*, 2014, **63**, p 245–248
9. R.N. Raoelison, T. Sapanathan, E. Padayodi et al., Interfacial Kinematics and Governing Mechanisms Under the Influence of High Strain Rate Impact Conditions: Numerical Computations of Experimental Observations, *J. Mech. Phys. Solids*, 2016, **96**, p 147–161
10. Shougo Kakizaki, Mitsuhiro Watanabe, and Shinji Kumai, Simulation and Experimental Analysis of Metal Jet Emission and Weld Interface Morphology in Impact Welding, *Mater. Trans.*, 2011, **52**(5), p 1003–1008
11. J. Nishiwaki, Y. Sawa, Y. Harada et al., SPH Analysis on Formation Manner of Wavy Joint Interface in Impact Welded Al/Cu Dissimilar Metal Plates, *Mater. Sci. Forum*, 2014, **794–796**, p 383–388
12. Yusuke Aizawa, Junto Nishiwaki, Yohei Harada et al., Experimental and Numerical Analysis of the Formation Behavior of Intermediate Layers at Explosive Welded Al/Fe, *J. Manuf. Process.*, 2016, **24**, p 100–106
13. Xiao Wang, Yuanyuan Zheng, Huixia Liu et al., Numerical Study of the Mechanism of Explosive/Impact Welding Using Smoothed Particle Hydrodynamics Method, *Mater Des.*, 2012, **35**, p 210–219
14. J.H. Wang, *Two-dimensional unsteady flow and shock wave*, Science Press, Beijing, 1994 (Chinese)
15. G.C. Sih, Thermomechanics of Nonequilibrium and Irreversible Processes (1), *Adv. Mech.*, 1989, **19**(2), p 158–171 (Chinese)
16. G.C. Sih, Thermomechanics of Nonequilibrium and Irreversible Processes (2), *Adv. Mech.*, 1989, **19**(3), p 304–319 (Chinese)
17. V.I. Lysak and S.V. Kuzmin, Energy Balance During Explosive Welding, *J. Mater. Process. Technol.*, 2015, **222**, p 356–364
18. Ali Nassiri, Greg Chini, Anupam Vivek et al., Arbitrary Lagrangian-Eulerian Finite Element Simulation and Experimental Investigation of Wavy Interfacial Morphology During High Velocity Impact Welding, *Mater. Des.*, 2015, **88**, p 345–358
19. I.A. Bataev, D.V. Lazurenko, S. Tanaka et al., High Cooling Rates and Metastable Phases at the Interfaces of Explosively Welded Materials, *Acta Mater.*, 2017, **135**, p 277–289
20. M.A. Meyers and K.K. Chawla, *Mechanical behavior of materials*, Camberidge University Press, Cambridge, 2009
21. Lili Liu, Yunfei Jia, and Fuzhen Xuan, Gradient Effect in the Waved Interfacial Layer of 304L/533B Bimetallic Plates Induced by Explosive Welding, *Mater. Sci. Eng. A*, 2017, **704**, p 493–502
22. M.M. Hoseini Athar and B. Tolaminejad, Weldability Window and the Effect of Interface Morphology on the Properties of Al/Cu/Al Laminated Composites Fabricated by Explosive Welding, *Mater. Des.*, 2015, **86**, p 516–525
23. S.A.A. Akbari Mousavi and P. Farhadi Sartangi, Experimental Investigation of Explosive Welding of cp-titanium/AISI, 304 Stainless Steel, *Mater. Des.*, 2009, **30**, p 459–468